A Procedure for Calculating Fields Inside Arbitrarily Shaped, Inhomogeneous Dielectric Bodies Using Linear Basis Functions with the Moment Method

CHI-TAOU TSAI, HABIB MASSOUDI, MEMBER, IEEE, CARL H. DURNEY, SENIOR MEMBER, IEEE, AND MAGDY F. ISKANDER, SENIOR MEMBER, IEEE

Abstract—**A moment method for calculating the internal field distributions of arbitrarily shaped, inhomogeneous dielectric bodies is presented. A free-space Green's function integral equation is used with 3-D linear basis functions to describe the field variation within cells. Polyhedral volume elements are used to model the scatterer's curvature realistically without an excessive number of unknowns. A new testing procedure, called the modified Galerkin's method, is developed and used to obtain the matrix equations with less CPU time but greater accuracy.**

Calculated internal field distributions of dielectric spheres, spheroids, and a composite model of a rat are compared with other calculations and experimental data. The agreement is generally good.

I. INTRODUCTION

THE CALCULATION of induced electromagnetic (EM) fields in irregularly shaped, inhomogeneous dielectric models of humans and biological systems is still a difficult problem in theoretical dosimetry [1]. Such calculations are important because knowledge of the internal field distributions can help identify potential local maxima of absorbed energy and avoid possible health hazards due to EM radiation that might occur even though the average absorption rate is below the hazardous level. A knowledge of absorbed energy patterns is also important in many applications such as hyperthermia, medical diagnostics, and antenna coupling.

The general procedure for calculating absorbed energy is to solve Maxwell's equations for the particular model representing the absorber. Exact determination of the induced internal field distributions of biological bodies is difficult because the solutions are strongly dependent upon such factors as shape, dimensions, internal structures of the bodies, and frequency of the incident wave. The finite-element method [2], [3] is best suited for bounded regions such as waveguides, but is difficult to use in problems involving radiation in unbounded space. Techniques using fast Fourier transforms (FFTs) have been successfully applied only to cylindrical scatterers [4]. The formulations of the surface-integral-equation technique (SIE) [5] and the extended-boundary-condition method (EBCM) [6] are general for arbitrarily shaped, inhomogeneous scatterers, and the EBCM has long been used to compute the average EM energy absorption rate of human bodies up to resonance frequencies [7]. Because of numerical complexity, however, only homogeneous objects with axisymmetric shapes have been tackled by these two methods.

A solution based on the method of moments [8] with cubical cells and pulse basis functions is applicable to arbitrarily shaped bodies with inhomogeneities [9]. A 180-cell inhomogeneous realistic model of man has been used with this method to calculate whole-body average specific absorption rates (SARs) for EM biohazard studies [10], and recent calculations for a 1132-cubical-cell model have also been reported [11]. Massoudi *et al.* [12], however, have shown that some serious deficiencies in this method make the accuracy of the calculated internal field distributions questionable. Basically, the numerical solutions obtained by this approach tend to diverge with respect to the subdivision of the cubical cells. A second moment-method-based technique suitable for field calculations inside arbitrarily shaped, inhomogeneous dielectric bodies has been developed recently by Schaubert *et al.* [13]. They have used tetrahedral volume elements combined with special vector basis functions (roof-top functions) in the moment-method solutions. The tetrahedral cells give better modeling flexibility; however, from the data presented in [13], it seems that this technique does not give greatly improved results over the pulse-basis-function method.

The technique described here is based on the method of moments and the use of a free-space Green's function integral equation (FGIE) similar to that given by Harrington [8] and others and suggested by Massoudi *et al.* [12] as being better for this application than the dyadic Green's function integral equation. The FGIE appears to offer some advantages in internal field distribution calculations because it includes an explicit expression of the

Manuscript received August 26, 1985; revised May 12, 1986. This work was supported in part by USAF School of Aerospace Medicine, Brooks Air Force Base, TX 78235 under Contract F33 615-82-C-0601.

C. T. Tsai, C. H. Durney, and M. F. Iskander are with the Electrical Engineering Department, University of Utah, Salt Lake City, UT 84112.

H. Massoudi was with the Electrical Engineering Department, University of Utah, Salt Lake City. He is now with Damaskos, Inc., Concordville, PA 19331.

IEEE Log Number 8610283.

0018-9480/86/1100-1131$01.00 ©1986 IEEE

electric surface charge density and is less singular than the dyadic Green's function integral equation commonly used with pulse basis functions. Subsectional 3-D linear basis functions are used to describe the field variation within each cell. In conjunction with the linear basis functions, polyhedral cells are used to model 3-D dielectric objects. This allows us to represent the curvature of the bodies more realistically with fewer cells.

We have developed a new testing procedure, called the modified Galerkin's method (MGM), to obtain the matrix equations from the FGIE. The new technique modifies the Galerkin's method in such a way that the volume-averaging integrations can be approximated analytically. This greatly reduces the amount of computation time required and makes calculations using linear basis functions practical for some models.

In the next section, the FGIE is described and the MGM testing procedure introduced. Numerical results based on these procedures are presented in Section III. Section IV discusses some possible approaches for improving the linear approximation method.

II. Formulations

A. The Electric-Field Integral Equation

Consider a lossy, inhomogeneous dielectric body exposed to the fields of an incident EM wave, as shown in Fig. 1. The total electric field $\boldsymbol{E}(\boldsymbol{r})$ at any point within the dielectric body can be expressed as

$$\boldsymbol{E}(\boldsymbol{r}) = \boldsymbol{E}^i(\boldsymbol{r}) + \frac{1}{4\pi}\int_{v'}(\epsilon_r(\boldsymbol{r}')-1)\boldsymbol{E}(\boldsymbol{r}')\frac{e^{-jR}}{R}\,dv' - \frac{1}{4\pi}\int_{v'}\{\nabla'\cdot[(\epsilon_r(\boldsymbol{r}')-1)\boldsymbol{E}(\boldsymbol{r}')]\}\cdot\frac{e^{-jR}}{R}\left(j+\frac{1}{R}\right)\hat{\boldsymbol{R}}\,dv' \tag{1}$$

where $\boldsymbol{r}$ is the position vector of the field point, $\boldsymbol{r}'$ is the position vector of the source point, both normalized to K,

$$R = |\boldsymbol{r}-\boldsymbol{r}'|$$

$$\hat{\boldsymbol{R}} = \frac{(\boldsymbol{r}-\boldsymbol{r}')}{|\boldsymbol{r}-\boldsymbol{r}'|}$$

ϵ_r is the complex permittivity of the body, and $\boldsymbol{E}^i(\boldsymbol{r})$ is the incident electric field. Note that (1) has been normalized with respect to k, the free-space propagation constant, and that an $e^{j\omega t}$ time dependence is assumed; hence, $\epsilon_r(\boldsymbol{r}')$ can be written as $\epsilon_r(\boldsymbol{r}') = \epsilon'(\boldsymbol{r}') - j\epsilon''(\boldsymbol{r}')$. The derivation of (1) is similar to derivations in [8]. Equation (1) is the FGIE suggested by Massoudi *et al.* [12] as a better integral equation for this method, and is equivalent to the one used by Schaubert *et al.* [13]. The second term on the right-hand side of (1) corresponds to the induced polarization current sources due to the incident wave, while the third term is the electric field produced by the induced charges in the dielectric body. For simplicity, we assume a constant $\epsilon_r(\boldsymbol{r}')$ in each cell and zero free charge density. At every point inside the cell except at the cell boundaries, the $\nabla'\cdot[(\epsilon_r(\boldsymbol{r}')-1)\boldsymbol{E}(\boldsymbol{r}')]$ becomes zero when using this assumption, and the third term on the right-hand side of (1) reduces to a surface integral. Therefore, the shape of cell boundaries is important in evaluating (1).

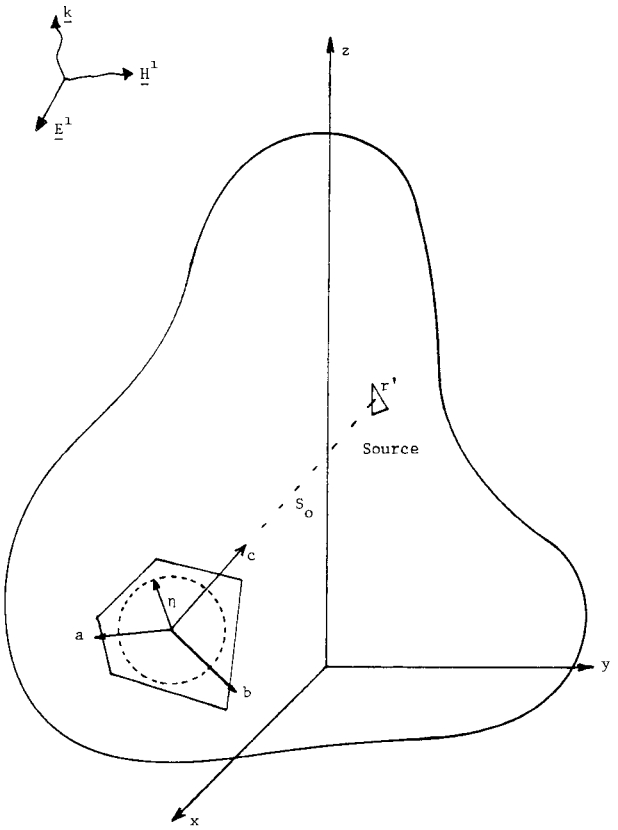

Fig. 1. The source point, the polyhedral cell with the mathematical averaging sphere, and the new coordinate system (a, b, c) for analytical evaluation of the Galerkin's averaging integrals.

B. Basis Functions

To solve for the unknown $\boldsymbol{E}(\boldsymbol{r})$ in (1), the irradiated object is partitioned into subsections, called cells, and the E field in each cell is expressed in terms of a set of basis functions. As mentioned before, solutions obtained with pulse basis functions have not been satisfactory. Hence, we have used linear subsectional basis functions to approximate the fields in each cell. The E field in cell n is approximated as

$$\boldsymbol{E}(\boldsymbol{r}_n) = \{[a_{nx}(x-x_n)+b_{nx}(y-y_n)+c_{nx}(z-z_n)+d_{nx}]\hat{\boldsymbol{i}} + [a_{ny}(x-x_n)+b_{ny}(y-y_n)+c_{ny}(z-z_n)+d_{ny}]\hat{\boldsymbol{j}} + [a_{nz}(x-x_n)+b_{nz}(y-y_n)+c_{nz}(z-z_n)+d_{nz}]\hat{\boldsymbol{k}}\}P_n \tag{2}$$

where $a_{nx}, b_{nx}, c_{nx}, d_{nx}, \cdots$ are unknown coefficients,

$\hat{i}, \hat{j}, \hat{k}$ are the unit vectors of the x, y, z rectangular coordinate system, and x_n, y_n, and z_n are the coordinates of the centroid of cell n. The P_n in (2) is defined as

$$P_n = \begin{cases} 1 & \text{if } \boldsymbol{r} \text{ is in cell } n \\ 0 & \text{otherwise.} \end{cases} \tag{3}$$

There are 12 unknowns for each cell, as can be seen from (2).

Tetrahedral cells can represent a curved surface more smoothly than cubical cells, but at the price of a larger number of cells. We have therefore found polyhedral cells to be better than tetrahedral cells because polyhedral cells can represent the surfaces better with a manageable number of unknowns. A good representation of the surfaces on which the surface charge density is present seems to be a critically important factor in the numerical calculations.

C. The Modified Galerkin's Method

A testing procedure that will generate a set of linear independent equations is needed for solving for the unknown coefficients in (2) using the method of moments. The point-matching technique is relatively simple, but its solution is usually unstable. It has been found that point-matching solutions are usually sensitive to the particular points used for matching; hence, they are not suitable for our purposes [8, pp. 11–14]. Galerkin's method, in which the solution is forced to satisfy the integral equation in an average sense over the whole cell, is considered to be more stable. Galerkin's method involves choosing the weighting (testing) functions to be the same as basis functions in the inner product of the method-of-moments solution as follows:

$$\langle \boldsymbol{w}, \boldsymbol{g} \rangle = \int_v \boldsymbol{w} \cdot \boldsymbol{g}\, dv = \int_{v_m} \boldsymbol{f} \cdot \boldsymbol{g}\, dv \tag{4}$$

where $\boldsymbol{w}$ and $\boldsymbol{f}$ are the weighting and basis functions, respectively, and this integration is over the whole volume of the dielectric. Because of (3), the integration limits of (4) actually can be reduced to v_m, the volume of the cell m where the weighting function $\boldsymbol{w}$ is defined.

We had first tried using Galerkin's method to calculate the fields inside a dielectric sphere irradiated by a plane wave in order to compare the calculated results with those of the exact Mie solution. Since the matrix elements cannot be evaluated in closed form, numerical integrations based on subdividing the polyhedrons were used to approximate (2) and (4) [15]. We found that in order to evaluate the matrix elements numerically with reasonable accuracy, large amounts of CPU time were required for models with relatively simple geometry. Therefore, it is difficult and impractical to apply this method with Galerkin's testing procedure to complicated objects such as biological bodies.

In order to overcome the drawback of Galerkin's method, i.e., excessive amounts of CPU time required for numerical integration, we have developed a new testing procedure, called the modified Galerkin's method (MGM), to obtain the N independent linear equations. The procedures of the MGM are as follows.

1) In the MGM, the weighting functions are chosen to be the same as the basis functions in Galerkin's method.

2) Instead of (4), the inner product of the MGM is defined as

$$\langle \boldsymbol{w}, \boldsymbol{g} \rangle = \int_{v_{sm}} \boldsymbol{w} \cdot \boldsymbol{g}\, dv = \int_{v_{sm}} \boldsymbol{f} \cdot \boldsymbol{g}\, dv \tag{5}$$

where v_{sm} is a mathematical sphere with radius η and center at the centroid of cell m where the weighting functions are defined. Note that v_m in (4) stands for the whole volume of cell m while, in the MGM, the volume is that of a sphere centered in the mth cell. As a result, the field representation in the MGM is forced to satisfy the integral equation over this mathematical sphere instead of over the whole cell.

3) Taking the inner product of weighting functions with (1) and rearranging terms, we have

$$\begin{aligned} &\int_{v_{sm}} \boldsymbol{w}(\boldsymbol{r}) \cdot \boldsymbol{E}(\boldsymbol{r})\, dv - \frac{1}{4\pi} \int_{v'} (\epsilon_r(\boldsymbol{r}') - 1) \boldsymbol{E}(\boldsymbol{r}') \\ &\qquad \cdot \left\{ \int_{v_{sm}} \boldsymbol{w}(\boldsymbol{r}) \frac{e^{-jR}}{R}\, dv \right\} dv' \\ &\qquad + \frac{1}{4\pi} \int_{v'} \{ \nabla' \cdot (\epsilon_r(\boldsymbol{r}') - 1) \boldsymbol{E}(\boldsymbol{r}') \} \\ &\qquad \cdot \left\{ \int_{v_{sm}} \frac{e^{-jR}}{R} \left(j + \frac{1}{R} \right) \boldsymbol{w}(\boldsymbol{r}) \cdot \hat{\boldsymbol{R}}\, dv \right\} dv' \\ &\quad = \int_{v_{sm}} \boldsymbol{w}(\boldsymbol{r}) \cdot \boldsymbol{E}^i(r)\, dv \end{aligned} \tag{6}$$

where $\boldsymbol{w}(\boldsymbol{r})$ is the weighting function. Note that the order of integration in the second and third terms on the right-hand side of (1) has been switched; namely, the Galerkin's averaging integrations are calculated first and the source integrations second.

4) Because v_{sm} is the volume of a mathematical sphere with radius η and center at the centroid of cell m, all the Galerkin's averaging integrations in (6) can be performed analytically to get closed-form expressions for these terms.

For example, substituting one of the $\boldsymbol{w}(\boldsymbol{r})$'s into (6), the Galerkin's averaging integral in the second term of (6), i.e., $\int_{v_{sm}} \boldsymbol{w}(\boldsymbol{r}) e^{-jR}/R\, dv$, will take one of the following scalar forms:

$$\begin{aligned} V_1(\boldsymbol{r}') &= \int_{v_{sm}} (x - x_n) \frac{e^{-jR}}{R}\, dv \\ V_2(\boldsymbol{r}') &= \int_{v_{sm}} (y - y_n) \frac{e^{-jR}}{R}\, dv \\ V_3(\boldsymbol{r}') &= \int_{v_{sm}} (z - z_n) \frac{e^{-jR}}{R}\, dv \\ V_4(\boldsymbol{r}') &= \int_{v_{sm}} \frac{e^{-jR}}{R}\, dv \end{aligned} \tag{7}$$

multiplied by a unit vector $\hat{i}$, $\hat{j}$, or $\hat{k}$. With reference to Fig. 1, we define a new coordinate system (a, b, c) with origin at the center of the mathematical sphere and with the c axis along the line joining the center of the sphere to a source point $\boldsymbol{r}'$. After the coordinate transformation and some trigonometric manipulation, the closed-form solutions of (7) can be written as

$$V_1(\boldsymbol{r}') = \alpha V_w(\boldsymbol{r}')$$
$$V_2(\boldsymbol{r}') = \beta V_w(\boldsymbol{r}')$$
$$V_3(\boldsymbol{r}') = \gamma V_w(\boldsymbol{r}')$$
$$V_4(\boldsymbol{r}') = \frac{4\pi e^{js_0}}{s_0}\{\sin(\eta) - \eta\cos(\eta)\}\hat{c} \tag{8}$$

with

$$V_w(\boldsymbol{r}') = \frac{\pi e^{-js_0}}{s_0^2}\{\sin(\eta)[-4\eta^2 + 12js_0 - 4js_0\eta^2 + 12] + \cos(\eta)[-12\eta - 12js_0\eta]$$

where $\alpha = \hat{i}\cdot\hat{c}$, $\beta = \hat{j}\cdot\hat{c}$, $\gamma = \hat{k}\cdot\hat{c}$, and s_0 is the distance between the center of the mathematical sphere and the source point $\boldsymbol{r}'$. Equations (8) are the various closed-form expressions for the Galerkin's averaging integral of the second term in (6). The averaging integrals in the other terms in (6) can be obtained in a similar way. Hence, (6) is reduced to

$$I - \frac{1}{4\pi}\int_{v'}(\epsilon_r(\boldsymbol{r}') - 1)\boldsymbol{E}(\boldsymbol{r}')\cdot\boldsymbol{V}(\boldsymbol{r}')\,dv' + \frac{1}{4\pi}\int_{v'}\{\nabla'\cdot(\epsilon_r(\boldsymbol{r}') - 1)\boldsymbol{E}(\boldsymbol{r}')\}S(\boldsymbol{r}')\,dv' = I^i \tag{9}$$

with

$$I = \int_{v_{sm}} \boldsymbol{w}(\boldsymbol{r})\cdot\boldsymbol{E}(\boldsymbol{r})\,dv$$
$$S(\boldsymbol{r}') = \int_{v_{sm}} (\boldsymbol{w}(\boldsymbol{r})\cdot\hat{\boldsymbol{R}})\frac{e^{-jR}}{R}\left(j + \frac{1}{R}\right)dv$$
$$\boldsymbol{V}(\boldsymbol{r}') = \int_{v_{sm}} \boldsymbol{w}(\boldsymbol{r})\frac{e^{-jR}}{R}\,dv$$
$$I^i = \int_{v_{sm}} \boldsymbol{w}(\boldsymbol{r})\cdot\boldsymbol{E}^i(\boldsymbol{r})\,dv.$$

The integrals of the second and third terms in (9) are evaluated numerically.

There are two main parameters in the MGM, namely, the position and the size of the mathematical averaging sphere in each cell. We can always put the center of this sphere close to the centroid of each cell so that the larger part of the cell is covered by the sphere. Based on the cases considered, a rule of thumb in choosing the radius η of this sphere is to make the volume of the cell equal to the volume of the averaging sphere. In this way, most of the cell will be enclosed in the sphere, and perhaps even part of the neighboring cells will be included. This should not cause a problem. If the assigned regional basis functions are able to describe the field variation within one cell reasonably well, requiring the basis functions to satisfy the integral equation over the volume of the averaging sphere would be a good approximation to requiring them to satisfy the integral equation over the volume of the entire cell. Since this is a least-square best fit of the basis functions in an average sense over a volume, the results would not be expected to depend critically on the exact definition of the volume. This is the basic idea behind the MGM.

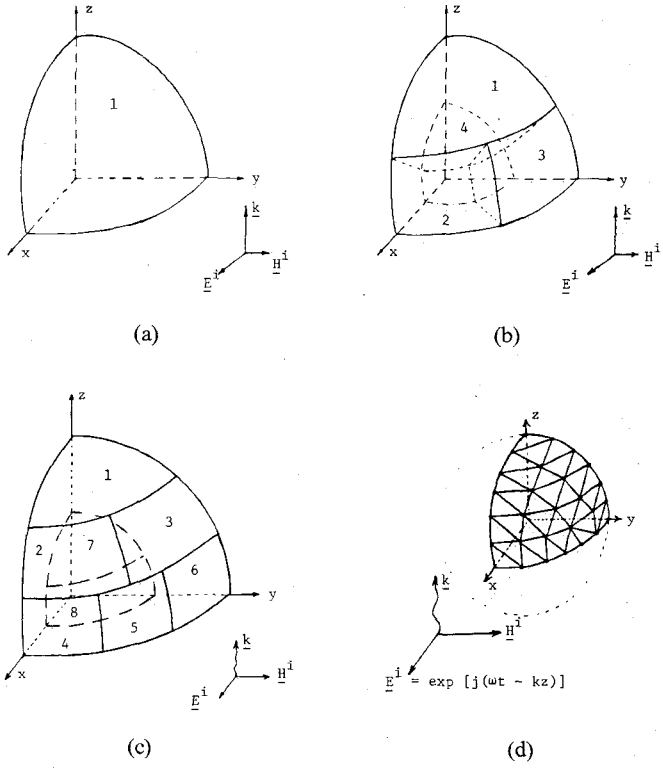

Fig. 2. Polyhedral cell models of one-eighth of a sphere. (a) Cell arrangement of eight-cell model. (b) Cell arrangement of 32-cell model. (c) Cell arrangement of 64-cell model. (d) Outer surface patches of the polyhedron model.

It is important to note that the MGM is not equivalent to using spherical cells because, in the MGM, the integration over the sources is still carried out over the polyhedral cells. Only the averaging integration in the testing procedure is carried out over the spherical volume.

III. Numerical Results

In order to test the accuracy of the solutions obtained by the free-space Green's-function, linear-basis, modified Galerkin's method (FGLMG), we have computed the internal fields in both homogeneous and layered spheres exposed to an incident plane wave. These data are compared below with the exact Mie solution [16], which is the only available analytical solution for 3-D objects. Calculations have also been made for spheroids and a composite rat model. As described below, the results agree well with those of other numerical techniques and they agree qualitatively with some experimental data.

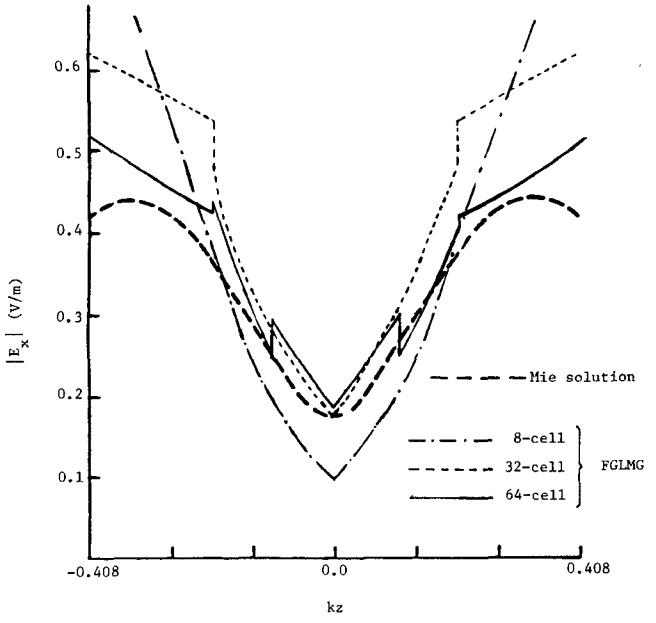

Fig. 3. Calculated E field along the z axis in a homogeneous dielectric sphere with $r_0 = 0.408/k$, $\epsilon_r = 36$, and $|E^i| = 1$ V/m. Eight-cell, 32-cell, and 64-cell models are used.

A. Spherical Objects

Three polyhedral models have been used to calculate the fields inside both homogeneous and layered dielectric spheres irradiated by an incident EM plane wave. Shown in Fig. 2(a)–(c) are one-eighth of the cell arrangements of eight-cell, 32-cell, and 64-cell polyhedral models, respectively. In the 32-cell model, there are four polyhedral cells in each octant of the dielectric sphere, with a total of four cells forming the core and 28 cells representing the shell. The 32-cell model and the 64-cell model are constructed in such a way that they can be used to model either a homogeneous sphere or a layered sphere.

The outer surface of the sphere is approximated by many small triangular patches on the polyhedral model, as shown in Fig. 2(d). Because there is no restriction on the number of patches a polyhedron can have, we have used up to 81 patches on one octant of a spherical surface, which constitutes a very realistic spherical model. These triangular patches are basic elements in the numerical calculation of the surface-charge term in (9). The volume integration terms in (9) are computed numerically using the ordinary rectangular rule, which consists of subdividing the polyhedral cells into small cubes and assuming a constant value in each cube. The cubes do not fit the boundaries of the polyhedral cells smoothly, but we have found that this is not very critical for the volume integral terms. The shape of the cells is critically important in evaluating the surface integral terms in (9), but not in evaluating the volume integral terms.

The first test case is a lossless, homogeneous dielectric sphere with a radius $r_0 = 0.408/k$ and permittivity $\epsilon_r = 36$ irradiated by an x-polarized EM plane wave propagating in the $+z$ direction. All three of the spherical models of Fig. 2 have been used to compute the induced E field for

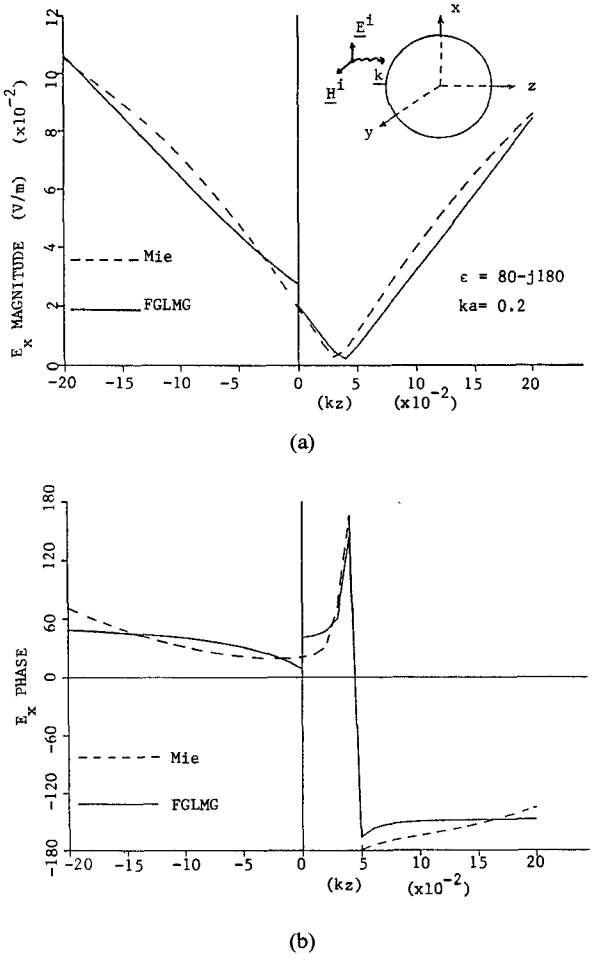

Fig. 4. Calculated E field along the z axis in an eight-cell model of a homogeneous, lossy dielectric sphere with $r_0 = 0.2/k$, $\epsilon_r = 80 - j180$, and $|E^i| = 1$ V/m. (a) Magnitude of E_x along the z axis. (b) Phase of E_x along the z axis.

comparison with the Mie solution. Fig. 3 shows the magnitude of the dominant field E_x along the z axis. It can be seen that increasing the number of mathematical cells in a given spherical model has systematically improved the accuracy of the numerical results; therefore, the calculated fields using this method appear to converge to the exact solution.

Fig. 4 shows the computed E fields along the z axis using the eight-cell spherical model and the Mie solution for a small but highly lossy homogeneous sphere. Both the magnitude and the phase of the fields have been plotted against kz. The worst error was less than 7 percent for the magnitude and 50 degrees for the phase. For most points, the error was less than 5 percent and 20 degrees for magnitude and phase, respectively.

The x component of the electric field along the z axis in a 32-cell model of a two-layered lossy dielectric sphere with a core radius $r_1 = 0.2/k$ with complex permittivity of $\epsilon_r = 40 - j40$ and an outer radius of $r_2 = 0.4/k$ with $\epsilon_r = 20 - j20$ is shown in Fig. 5. Data obtained from the Mie solution are also shown. The calculated fields can be seen to agree well with the analytical solution except at one end point, which has a maximum error of about 15 percent.

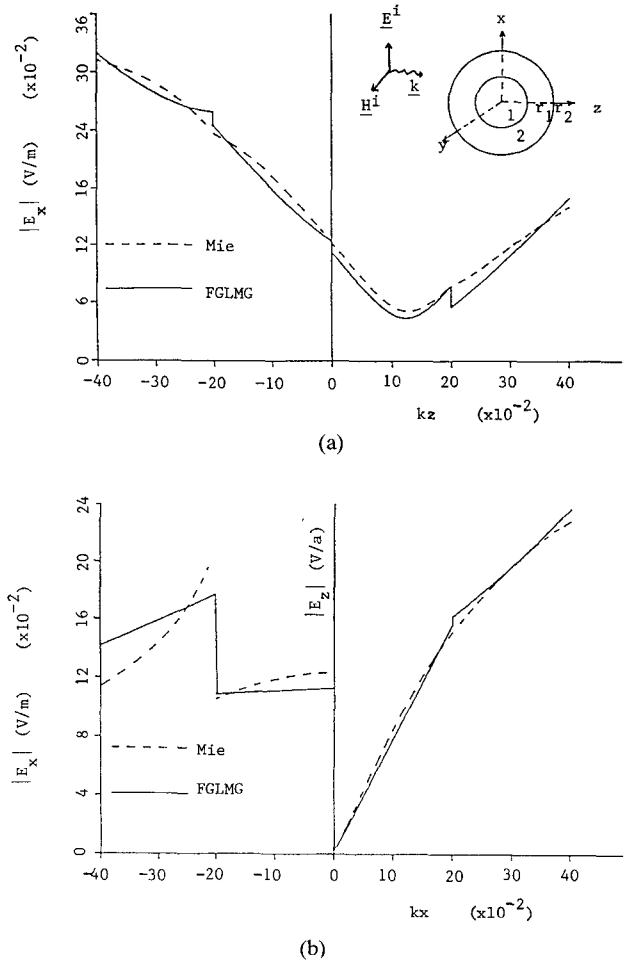

Fig. 5. Calculated E field along the z axis in a 32-cell model of a two-layered lossy dielectric sphere with $r_1 = 0.2/k$, $r_2 = 0.4/k$, $\epsilon_{r1} = 40 - j40$, $\epsilon_{r2} = 20 - j20$, and $|E^i| = 1$ V/m. (a) Magnitude of E_x along the z axis. (b) Magnitude of E_x and E_z along the x axis.

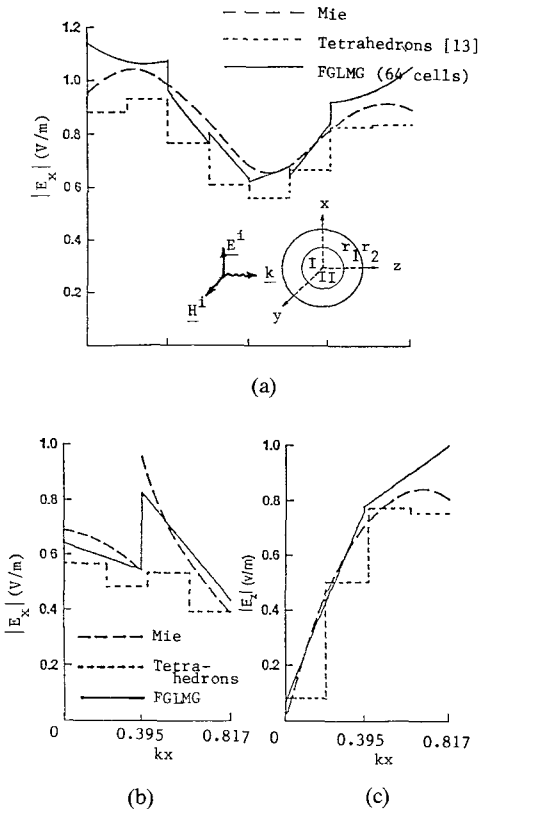

Fig. 6. Calculated E field along the z axis in a 64-cell model of a two-layered lossless dielectric sphere with $r_1 = 0.395/k$, $r_2 = 0.817/k$, $\epsilon_{r1} = 16$, $\epsilon_{r2} = 9$, and $|E^i| = 1$ V/m. (a) Magnitude of E_x along the z axis. (b) Magnitude of E_x along the x axis. (c) Magnitude of E_z along the x axis.

The fields inside a lossless dielectric layered sphere with a larger radius ($r_2 = 0.814/k$) have also been calculated using the 64-cell model. Fig. 6(a) is a plot of $|E_x|$ along the z axis; Fig. 6(b) and (c) show $|E_x|$ and $|E_z|$ along the x axis. Also shown are the results obtained by the exact Mie solution and by Schaubert *et al.* [13], who used tetrahedral cells with special (roof-top) basis functions and Galerkin's testing procedure.

The FGLMG shows a better agreement with the analytic solution than the tetrahedral solution, as indicated in Fig. 6(b). In the vicinity of the dielectric interface, the value of $|E_x|$ has a discontinuity because E_x is normal to the dielectric interface. The linear basis functions clearly reflect the discontinuity. The discontinuity is also implicit in the formulation using roof-top basis functions, but is not identifiable in the results shown in [13]; this is because the cell surfaces are not perpendicular to E_x, even though the spherical surface is. In the 64-polyhedral-cell model used with the linear basis functions, the number of unknowns can be reduced to 192 by taking advantage of two planes of symmetry. In the 512-cell tetrahedral model used with the roof-top basis functions, the number of unknowns can be reduced to 272 by using two planes of symmetry. Thus, the linear basis functions, in addition to requiring fewer unknowns, provide a smoother approximation than the roof-top functions, since the latter are linear in only one direction.

The electric-field boundary condition requires the parallel component to be continuous at the interface of inhomogeneities. Because of the use of subsectional basis functions, discontinuities usually appear at the cell boundaries of the solutions. This can be observed clearly in Fig. 3 and Fig. 6(a) and (c), where the exact solutions predicted a continuous curve, but the linear basis approximation showed some jumps at the cell boundaries. Since these jumps point out the degree of discrepancy between the linear approximation and the exact solution, they can be used as an important guide. When applying the FGLMG to an unknown problem, if the resultant jumps are small compared with the total field, the calculated solution is probably close to the exact solution. If, however, the jumps appear to be large, the results obtained on the cell boundaries are contradictory and the calculated fields are probably incorrect. This would indicate that smaller cells must be used to obtain more accurate results.

B. Nonspherical Objects

The FGLMG has also been used to compute the induced E field inside nonspherical bodies exposed to the fields of an EM plane wave. A homogeneous spheroidal model consisting of 24 polyhedral cells with 72 unknowns (using two planes of symmetry) has been used with the

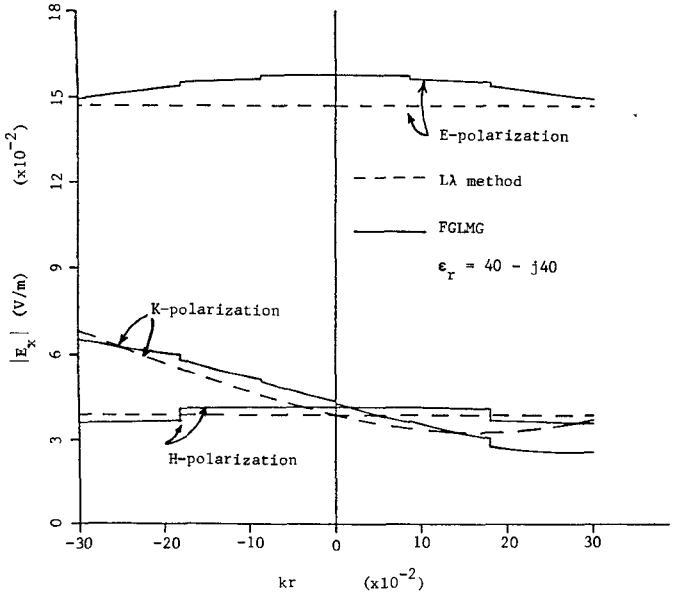

Fig. 7. Calculated E field along the major axis in a model of a lossy dielectric spheroid, $|E^i| = 1$ V/m, by the linear-basis-function method and the long-wavelength approximation. Three major cases (E, H, and K polarization) are shown.

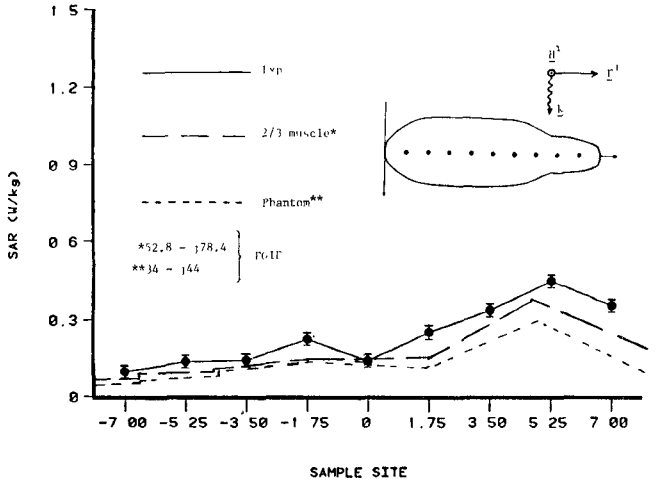

Fig. 8. SAR distribution inside a composite model of a medium-size rat irradiated by an EM plane wave at 360 MHz; E polarization. The model is 17.5 cm long and 5.2 cm wide.

linear-basis-function method. The calculated data have been compared with those obtained by the long-wavelength analysis [17]. Data for three standard polarizations, E, H, and K, are shown in Fig. 7 for a spheroid of $ka = 0.3$, $a/b = 3$, and $\epsilon_r = 40 - j40$, where a and b are the semimajor and semiminor axes, respectively. The agreement of these two techniques appears to be very good.

An ongoing research project at the University of Utah has been the experimental determination of the SAR distribution in models of a rat exposed to EM fields in the range of 360 MHz to 2450 MHz. One of the models is a composite of two prolate spheroids, one simulating the head and the other the body of a medium-size rat with a total length of 17.5 cm and a mass of 256 g [18]. This model was made of material with electric properties of muscle and was irradiated by a 360-MHz plane-wave source.

The experimental SAR data shown in Fig. 8 were taken from nine temperature probes placed along the major axis of the composite rat model. Some preliminary data on SAR distributions inside this composite model using the linear-basis-function method have been obtained and compared with the experimental data. Since the actual permittivity of the model material has not yet been measured, the calculated SAR distributions for two different values of complex permittivity, along with the experimental data, are shown in Fig. 8. Reasonably good qualitative agreement for the calculated and the measured data can be observed in Fig. 8.

C. Computation Time

The calculations with linear basis functions described above were made on the University of Utah's Univac 1161 computer. The CPU time consumed depended upon the number of cells, the cell configuration, and the degree of accuracy required. For the results of Fig. 3 obtained with eight-cell, 32-cell, and 64-cell spherical models, the CPU times were 2.6 min, 8 min, and 47 min, respectively. These times include tracing the triangular patches, building the matrix, and doing LU factorization. It has been found that most of the computation time, about 90 percent, was spent on filling the matrix, which includes two numerical integrations as in (9).

We have found that particularly the second term (volume integral) in (9) accounts for most of the matrix building time because it is based on a crude algorithm. In all the cases described above, the numerical integrations have been overdone to ensure accuracy.

In other words, similar results should still be obtained with less accuracy in evaluating the matrix elements and hence less CPU time. For larger objects, such as the case of Fig. 6, we have used more subdivisions in numerical integration, so the total CPU time was as high as 81 min. One thing worth mentioning is that the $(\epsilon_r(\boldsymbol{r}') - 1)$ term in (9) can be decoupled from the matrix. Therefore, the matrix for a specific cell geometry at a given frequency can be first built and stored, and the results for different dielectric constants but the same shape and size can be obtained by repeatedly inverting the stored matrix coupled back with factors $(\epsilon_r(\boldsymbol{r}') - 1)$. Considerable savings in computation time can be achieved in this way because the matrices need only be built once.

IV. Discussion and Summary

A new method for computing the induced electromagnetic fields inside arbitrarily shaped, three-dimensional, inhomogeneous dielectric bodies has been presented. This method is based on the use of arbitrarily shaped polyhedral volume elements, which allows realistic modeling of body shapes.

Subsectional linear basis functions have been used to represent the field within each cell. Although these basis functions result in larger matrices for a given number of cells than pulse basis functions, the cell size can generally

be much larger with linear basis functions than with pulse functions. The 3-D linear basis functions also provide a smoother description of the fields.

A new testing procedure, called the modified Galerkin's method, has been developed and used with the method-of-moments solution. The advantages of the MGM testing procedures over the ordinary Galerkin's method can be summarized as follows.

1) It replaces the numerical integration for averaging over the cells by analytical integrations over spheres approximating the cell volumes, which greatly reduces computation time and numerical errors.

2) It eliminates the troublesome $1/R$ singularity in the self-term of Galerkin's method.

3) Because the numerical averaging integration is omitted, multipatched polyhedrons can be used to form a very realistic model.

A major limitation of the linear basis functions is the large matrices required for a given number of cells as compared to other methods. The condition $\nabla' \cdot [(\epsilon_r(\boldsymbol{r}') - 1)\boldsymbol{E}(\boldsymbol{r}')] = 0$ in the internal region of every cell, as discussed above, can be applied to reduce further the number of unknowns per cell by one. However, 11 unknowns per cell is still large compared with the three unknowns in each cell for pulse basis functions. A possible way to reduce the number of unknowns required for the linear basis functions would be to require the basis functions in each cell to satisfy the boundary conditions at the cell walls. This, of course, would also complicate the algorithms. The technique, however, does appear promising; in the one test case we tried, we found that the calculated results were about the same when the number of unknowns was reduced by satisfying the boundary conditions as when the boundary conditions were not used [15]. In order to reduce the CPU time required to build the matrices, the primitive rectangular rule used in evaluating the numerical integrations should also be replaced by a more efficient algorithm.

Test cases including homogeneous spheres, layered spheres, and nonspherical objects indicate that better accuracy in calculating internal SAR distributions can be obtained by using linear basis functions. In order to increase the applicable range of this method, for instance, to larger and more complex dielectric bodies such as human bodies, more work needs to be done in reducing the unknowns in each cell so that more cells can be used in modeling the complex structures.

ACKNOWLEDGMENT

The authors thank Dr. J. A. D'Andrea for providing the measured data.

REFERENCES

[1] C. H. Durney, "Electromagnetic dosimetry for models of humans and animals: A review of theoretical and numerical techniques," *Proc. IEEE*, vol. 68, no. 1, pp. 33–40, Jan. 1980.

[2] B. H. McDonald and A. Wexler, "Finite element solution of unbounded problems," *IEEE Trans Microwave Theory Tech.*, vol. MTT-20, pp. 841–847, 1972.

[3] M. A. Morgan and K. K. Mei, "Finite element computation of scattering by inhomogeneous penetrable bodies of revolution," *IEEE Trans. Antennas Propagat.*, vol. AP-27, pp. 202–214, Mar. 1979.

[4] R. Kastner and R. Mittra, "A spectral-iteration technique for analyzing scattering from arbitrary bodies, Part I: Cylindrical scatterers with E-Wave incidence," *IEEE Trans. Antennas Propagat.*, vol. AP-31, pp. 499–506, May 1983.

[5] T. K. Wu and L. L. Tsai, "Scattering from arbitrarily-shaped lossy dielectric bodies of revolution," *Radio Sci.*, vol. 12, pp. 709–718, Sept. 1977.

[6] V. K. and V. V. Varadan, Eds., *Acoustic, Electromagnetic, and Elastic Wave Scattering — Focus on the T-Matrix Approach*. New York: Pergamon Press, 1980.

[7] C. H. Durney *et al.*, *Radiofrequency Radiation Dosimetry Handbook*, 2nd ed., USAF School of Aerospace Medicine, Brooks AFB, TX, Rep. SAM-TR-78-22, May 1978.

[8] R. H. Harrington, *Field Computations by Moments Methods*. New York: McGraw-Hill, 1968.

[9] D. E. Livesay and K-M Chen, "Electromagnetic fields induced inside arbitrarily shaped biological bodies," *IEEE Trans. Microwave Theory Tech.*, vol. MTT-22, pp. 1273–1280, Dec. 1974.

[10] M. J. Hagmann, O. P. Gandhi, and C. H. Durney, "Numerical calculation of electromagnetic energy deposition for a realistic model of man," *IEEE Trans. Microwave Theory Tech.*, vol. MTT-27, pp. 804–809, Sept. 1979.

[11] J. F. Deford, O. P. Gandhi, and M. J. Hagmann, "Moment-method solutions and SAR calculations for inhomogeneous models of man with large number of cells," *IEEE Trans. Microwave Theory Tech.*, vol. MTT-31, pp. 848–851, Oct. 1983.

[12] H. Massoudi, C. H. Durney, and M. F. Iskander, "Limitations of the cubical block model of man in calculating SAR distributions," *IEEE Trans. Microwave Theory Tech.*, vol. MTT-32, pp. 746–752, Aug. 1984.

[13] D. H. Schaubert, D. R. Wilton, and A. W. Glisson, "A tetrahedral modeling method for electromagnetic scattering by arbitrarily shaped inhomogeneous dielectric bodies," *IEEE Trans. Antennas Propagat.*, vol. AP-32, no. 1, pp. 77–85, Jan. 1984.

[14] S. C. Hill, C. H. Durney, and D. A. Christensen, "Numerical calculations of low-frequency TE fields in arbitrary shaped inhomogeneous lossy dielectric cylinders," *Radio Sci.*, vol. 18, pp. 328–336, May–June 1983.

[15] C. T. Tsai, "Numerical calculations of field distributions in 3-D, arbitrary shaped inhomogeneous dielectric objects using the method of moments with linear basis functions," Ph.D. dissertation, Elec. Eng. Dep., Univ. of Utah, 1985.

[16] J. A. Stratton, *Electromagnetic Theory*. New York: McGraw-Hill, 1941.

[17] H. Massoudi, C. H. Durney, and C. C. Johnson, "Long-wavelength electromagnetic power absorption in ellipsoidal models of man and animals," *IEEE Trans. Microwave Theory Tech.*, vol. MTT-25, pp. 47–52, Jan. 1977.

[18] J. A. D'Andrea, H. Massoudi, C. H. Durney, and M. F. Iskander, "Microwave radiation absorption within spheres and models of the medium-sized rat," presented at the 6th Annual Conference, Bioelectromagnetic Society, Atlanta, GA, July 15–19, 1984.

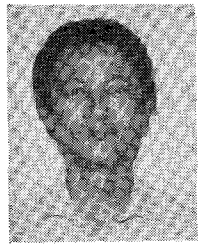

Chi-Taou Tsai was born in Taipei, Taiwan, on March 16, 1954. He received the B.S. degree in physics from the National Central University, Taiwan, in 1976. In 1983 and 1984, he obtained, respectively, the M.S. degree and the Ph.D. degree from the University of Utah, Salt Lake City, both in electrical engineering.

From 1979 to 1984, he was a graduate student in the Department of Electrical Engineering, University of Utah. His research interests included numerical electromagnetics, microwave biological effects, scattering and diffraction of electromagnetic waves, and microwave hyperthermia. Since graduating from the University of Utah, he has been employed as a senior staff engineer in the Semiconductor R/D Laboratories of Motorola Inc., Phoenix, AZ.

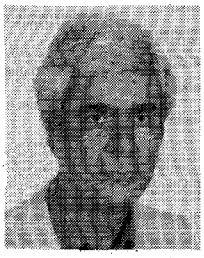

Habib Massoudi (S'74–M'76) received the B.Sc. degree from Teacher's Training University, Tehran, Iran, in 1964 and the M.Sc. degree from the University of Tehran, Tehran, Iran, in 1970, both in physics. Continuing his graduate studies at the University of Utah, Salt Lake City, he received the Ph.D. degree in electrical engineering in 1976.

He worked as a physics instructor in Iran from 1964 to 1970. From 1976 to 1985 he was with the University of Utah, where he was engaged in research in electromagnetic radiation, scattering, and interaction with biological systems. While at Utah, he also taught a graduate course on methods in electromagnetic wave propagation. His last rank at the University of Utah was that of Research Associate Professor of electrical engineering. Since August 1985, he has been with N. J. Damaskos, Inc., Concordville, PA, where he is engaged in research and development in projects related to electromagnetic scattering and radiation.

✠

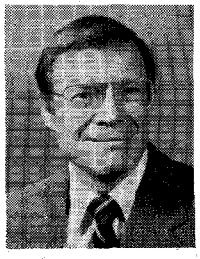

Carl H. Durney (S'60–M'64–SM'80) was born in Blackfoot, ID, on April 22, 1931. He received the B.S. degree in electrical engineering from Utah State University in 1958, and the M.S. and Ph.D. degrees in electrical engineering from the University of Utah in 1961 and 1964, respectively.

From 1958 to 1959, he was employed as an Associate Research Engineer with the Boeing Airplane Company, Seattle, WA, where he studied the use of delay lines in control systems. He has been with the University of Utah since 1963, when he was appointed Assistant Research Professor of Electrical Engineering. From 1965 to 1966, he was employed at the Bell Telephone Laboratories, Holmdel, NJ, while on leave from the University of Utah. During this time, he worked in the area of microwave avalanche diode oscillators. In 1971, Dr. Durney was engaged in study and research involving microwave biological effects at the University of Washington while on leave from the University of Utah. From 1977 to 1982, he was chairman of the Electrical Engineering Department at the University of Utah. While on sabbatical leave from the University of Utah during the 1983–84 academic year, he was Visiting Professor at the Massachusetts Institute of Technology, where he was engaged in research in nuclear magnetic resonance imaging and hyperthermia for cancer therapy. He is presently Professor of Electrical Engineering and Professor of Bioengineering at the University of Utah, where he is teaching and doing research in electromagnetics, engineering pedagogy, electromagnetic biological effects, and medical applications of electromagnetics.

Dr. Durney is a member of the Bioelectromagnetics Society, Commission B of URSI (International Union of Radio Science), Sigma Tau, Phi Kappa Phi, Sigma Pi Sigma, Eta Kappa Nu, and the American Society for Engineering Education. He also served as Vice-President (1980–81) and President (1981–82) of the Bioelectromagnetics Society. Dr. Durney is a member (1979–present) and was Chairman (1983–1984) of the IEEE Committee on Man and Radiation (COMAR), a member of the American National Standards Institute C95 Subcommittee IV on Radiation Levels and/or Tolerances with Respect to Personnel (1973–present), a member of the editorial board of the IEEE TRANSACTIONS ON MICROWAVE THEORY AND TECHNIQUES (1977–present), and a member of the editorial board of *Magnetic Resonance Imaging* (1982–present). In 1983, he coedited a special issue of the *Journal of Microwave Power* on "Electromagnetic techniques in medical diagnosis and imaging." In 1980, Dr. Durney received the Distinguished Research Award from the University of Utah, and the Outstanding Teaching Award, College of Engineering, University of Utah. In 1982, he received the American Society for Engineering Education Western Electric Fund Award for excellence in teaching and the Utah Section IEEE Technical Achievement Award. He was named a College of Engineering Distinguished Alumnus by Utah State University in 1983.

✠

Magdy F. Iskander (S'72–M'76–SM'84) was born in Alexandria, Egypt, on August 6, 1946. He received the B.Sc. degree in electrical engineering from the University of Alexandria, Egypt, in 1969. He entered the Faculty of Graduate Studies at the University of Manitoba, Winnipeg, Canada, in September 1971 and received the M.Sc. and Ph.D. degrees in 1972 and 1976, respectively, both in microwaves.

In 1976, he was awarded a National Research Council of Canada Postdoctoral Fellowship at the University of Manitoba. Since March 1977, he has been with the Department of Electrical Engineering and the Department of Bioengineering at the University of Utah, Salt Lake City, where he is currently a Professor of Electrical Engineering and Research Professor of Materials Science and Engineering. In 1981, he received the University of Utah President David P. Gardner Faculty Fellow Award and spent the academic quarter on leave as a Visiting Associate Professor at the Department of Electrical Engineering and Computer Science, Polytechnic Institute of New York, Brooklyn. In 1985, he spent the summer at Chevron Oil Field Research Company, La Habra, CA, as a visiting scientist.

Dr. Iskander edited two special issues of the *Journal of Microwave Power*, one on "Electromagnetics and energy applications," (March 1983), the other on "Electromagnetic techniques in medical diagnosis and imaging," (September 1983). He has contributed chapters to four research books and has published in technical journals and presented more than 140 papers. His present fields of interest include the use of numerical techniques in electromagnetics to calculate scattering by dielectric objects, antenna design, and the evaluation of the biological effects as well as the development of medical applications of electromagnetic energy. In 1983, Dr. Iskander received the College of Engineering Outstanding Teaching Award and the College Patent Award for creative, innovative, and practical invention. In 1984, he was selected by the Utah Section of IEEE as the Engineer of the Year. In 1984, he received the Outstanding Paper Award from the International Microwave Power Institute. In 1985, he received the Curtis W. McGraw ASEE National Research Award for outstanding early achievements by a university faculty member. He is a member of the editorial board of the IEEE TRANSACTIONS ON MICROWAVE THEORY AND TECHNIQUES and a member of the editorial board of the *Journal of Microwave Power*.